THE JOURNAL OF PHYSICAL CHEMISTRY C

Article

Cite This: J. Phys. Chem. C 2018, 122, 13529−13539

pubs.acs.org/JPCC

Direct Interfacial Electron Transfer from High-Potential Porphyrins into Semiconductor Surfaces: A Comparison of Linkers and Anchoring Groups

Jianbing Jiang,[†] Jacob A. Spies,[†] John R. Swierk, Adam J. Matula, Kevin P. Regan, Neyen Romano, Bradley J. Brennan,[‡] Robert H. Crabtree,* Victor S. Batista,* Charles A. Schmuttenmaer,* and Gary W. Brudvig*

Department of Chemistry, Yale University, New Haven, Connecticut 06520, United States

Energy Sciences Institute, Yale University, West Haven, Connecticut 06516, United States

Supporting Information

ABSTRACT: This study probes a series of linkers and anchoring groups for direct interfacial electron transfer (IET) from high-potential porphyrins into semiconductor surfaces. Eight different linker−anchor combinations of CF_3-substituted, high-potential porphyrins were designed, synthesized, and characterized. Specifically, a series of four anchors was examined (carboxylate, hydroxamate, phosphonate, and silatrane), along with two different linkers (phenylene and benzanilidylene), which differ in terms of their electronic conjugation and overall length. The electrochemical and photophysical properties of the porphyrins were evaluated by steady-state and transient spectroscopies in solution and on mesoporous SnO_2 substrates for use as dye photosensitizers in aqueous photoelectrochemical cells. IET dynamics were measured using time-resolved terahertz (TRTS) and transient absorption spectroscopies. From TRTS measurements, injection yields were determined relative to a commonly used phosphonated ruthenium(II) polypyridyl complex, which is reported to have near quantitative injection yield. We find that IET occurs through space rather than through the linkers, due to the tilted orientation of the adsorbed porphyrins in direct contact with the metal oxide surface. As a result, the anchoring groups have a less significant effect on IET dynamics than for adsorbates exhibiting through-linker injection. Experiments are supported by DFT calculations, including the analysis of different electron-injection pathways. Direct IET offers the advantage of the selection of anchoring groups based solely on chemical/photoelectrochemical stability and synthetic viability, irrespective of the electronic coupling of the anchoring group to the metal oxide surface.

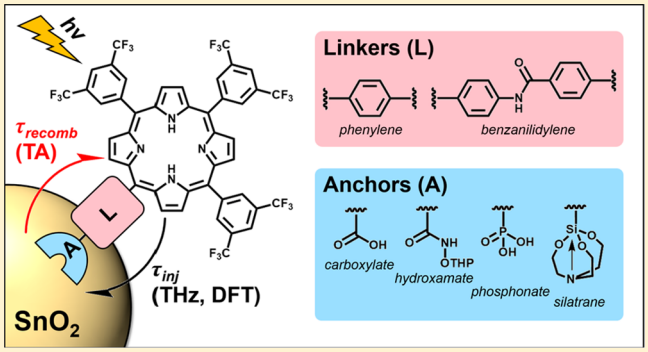

INTRODUCTION

Rising global energy demand and greenhouse gas emissions from burning fossil fuels have resulted in an increased interest in developing cost-effective, renewable energy resources.[1] Solar energy technologies that are efficient and comprise earth-abundant materials are at the forefront of renewable energy research. Solar energy technologies can be broadly categorized into those that generate electricity such as silicon-based photovoltaics,[2,3] dye-sensitized solar cells (DSSCs),[4−6] and perovskite solar cells[7−9] and those that generate a reduced chemical fuel using solar energy[10−13] (e.g., dihydrogen (H_2)[14−16] or methanol[17,18]). Solar fuel provides energy storage that can later be harnessed to produce electricity, or useful work.

Water-splitting dye-sensitized photoelectrochemical cells (WS-DSPECs)[19−21] utilize molecular chromophores and catalysts to produce H_2 under illumination. A typical WS-DSPEC drives water oxidation at a photoanode and proton reduction to generate H_2 at a dark cathode, though other examples of WS-DSPECs using photocathodes have been reported.[22−25] Because water oxidation is kinetically and thermodynamically challenging, considerable effort has been put into photoanode development. A typical WS-DSPEC photoanode consists of molecular photosensitizers and water-oxidation catalysts supported on a mesoporous metal oxide substrate, such as nanostructured TiO_2 or SnO_2. Photoexcitation of the molecular photosensitizer and subsequent electron injection into the metal oxide yields an electron in the conduction band of the metal oxide and a hole on the photosensitizer. The electron in the conduction band can then

Special Issue: Prashant V. Kamat Festschrift

Received: December 17, 2017
Revised: February 12, 2018
Published: February 12, 2018

DOI: 10.1021/acs.jpcc.7b12405
J. Phys. Chem. C 2018, 122, 13529−13539

travel to a transparent back contact and be shuttled to the cathode where proton reduction generates H_2. The hole on the oxidized photosensitizer moves across the surface via intermolecular hole transfer until encountering a water-oxidation catalyst, where water oxidation occurs.[20,21,26−28] Regarding the energetics of the photoanode in WS-DSPECs, the photosensitizer needs a ground-state potential that is sufficiently positive to oxidize a water-oxidation catalyst and an excited-state potential more negative than that of the semiconductor conduction band to facilitate interfacial electron transfer (IET).[29]

Options for photosensitizers in WS-DSPECS are more limited than traditional DSSCs, because the photosensitizers must be stable under oxidative conditions in an aqueous electrolyte.[30] The most commonly used photosensitizers are phosphonated ruthenium(II) polypyridyl dyes, but there is rising interest in porphyrins and other organic dyes to circumvent the need for ruthenium, a precious metal.[22,31−33] Porphyrins are of particular interest, because they have a highly tunable, broad absorption across the visible region and highest occupied molecular orbital (HOMO) levels that can be modulated to facilitate hole transfer to a water-oxidation catalyst.[32,34] In addition, synthetic strategies for modifying porphyrins have been widely studied, allowing for photophysical, electrochemical, and structural properties to be readily tuned.[35−41] However, selecting suitable linkers and anchoring groups for efficient electronic coupling with the semiconductor surface is challenging, particularly when IET requires suitable energy level alignment.

In this work, a series of eight high-potential, CF_3-substituted porphyrins with different linkers and anchoring groups (see Chart 1) were designed, synthesized, and characterized when attached to semiconductor surfaces using spectroscopic and theoretical methods. This class of high-potential porphyrins utilizes electron-withdrawing 3,5-bis-CF_3-substituted phenyl groups at the *meso* positions of the porphyrin ring to tune the ground- and excited-state potentials while avoiding the sensitivity to nucleophilic substitution of the *para*-fluoro substituent common with pentafluorophenyl groups.[34] Specifically, the influence of anchor and linker on IET dynamics and injection yield was studied. Variation of linkers and anchors is a common molecular design strategy to optimize photosensitizers for DSSCs and WS-DSPECs.[42,43] Four of the porphyrins bear a phenylene linker (**Ph**) but differ in the anchoring group: carboxylate (**Carb**), hydroxamate (**Hydrox**), phosphonate (**Phos**), or silatrane (**Sila**). The other four porphyrins have longer benzanilidylene linkers (**Bzd**) and the same series of anchors. The electrochemical, photophysical, and IET properties were studied by steady-state absorption and emission spectroscopies as well as time-resolved transient absorption (TA) and terahertz (THz) spectroscopies. DFT calculations were also performed to evaluate the injection pathway between the porphyrin and metal oxide.

Overall, our results challenge the commonly accepted view that the anchoring group significantly influences IET characteristics.[42−45] Our combined experimental and theoretical study demonstrates that the anchor group exerts little influence on the IET characteristics of molecular chromophores unless it is unusually highly coupled to the excited state of the chromophore. We find that through-space IET is the most likely scenario because the through-linker IET pathway is energetically inaccessible, and similar porphyrins adsorb to the surface with different tilt angles depending on the linker and anchor (making the IET pathway through space shorter by moving the porphyrin donor states closer to metal oxide acceptor states).[46] These results imply that the choice of anchoring group may be based primarily on chemical/photoelectrochemical stability and ready synthetic availability rather than perceived IET advantages of the anchoring group in such systems.

Chart 1. Series of CF_3-Substituted Porphyrins Investigated in This Work

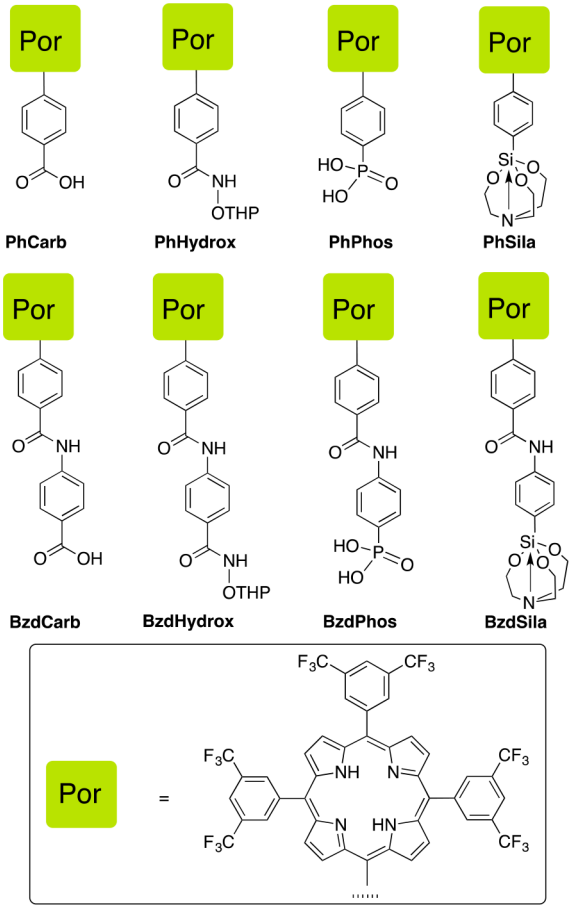

■ EXPERIMENTAL SECTION

Porphyrin Characterization. ^{1}H NMR spectra were recorded on an Agilent 400 MHz NMR instrument in $CDCl_3$ unless otherwise noted. Chemical shifts are reported as ppm from the internal reference tetramethylsilane. Absorption spectra were recorded on a Varian Cary 50 Bio UV−visible spectrophotometer. Fluorescence emission spectra were recorded on a Horiba Scientific FluoroMax Plus Fluorophotometer. The mass spectral data were obtained from a Thermo Scientific LTQ Orbitrap ELITE mass spectrometer. The sample was directly infused into the mass spectrometer via a syringe pump at 5 μL/min. 4-boronic ester-phenylsilatrane (**1**),[47] 4-aminophenylsilatrane (**2**),[47] **PhCarb**,[34] and **PhPhosEster**[34] were prepared according to reported procedures. The synthesis and characterization of the other compounds shown in Chart 1 are given in the Supporting Information.

Time-Resolved THz Spectroscopy (TRTS). The spectrometer and experimental method used for TRTS measurements are described in detail elsewhere.[48,49] Briefly, the 800 nm fundamental of a chirped-pulse, regeneratively amplified

DOI: 10.1021/acs.jpcc.7b12405
J. Phys. Chem. C 2018, 122, 13529−13539

Ti:sapphire laser (Spectra Physics Spitfire Ace, 35 fs pulse width, 1 kHz repetition rate) was split into three beams for THz generation, detection, and photoexcitation, respectively. The THz generation beam was frequency doubled, and the second harmonic and fundamental were focused to generate an air plasma.[50,51] The generated THz pulse was collimated and focused using off-axis paraboloidal mirrors and was detected via free-space electro-optic sampling in a ZnTe (110) crystal using the aforementioned detection beam.[52] The photoexcitation pump beam was frequency doubled to 400 nm and attenuated to 100 mW cm^{-2} (100 μJ cm^{-2} $pulse^{-1}$, 4 mm diameter spot) using a variable neutral density filter. The 800 nm fundamental was filtered out using dichroic mirrors. The time delay between the photoexcitation pump pulse and THz pulse was controlled using a mechanical delay stage.

TRTS measurements were fit using a multiexponential function

$$\Delta\mathrm{THz} = \left\{\sum_{i=1}^{n} A_i\left[\exp\left(-\frac{t}{\tau_i}\right) - 1\right]\right\} \otimes G_R \tag{1}$$

where n is the number of exponentials included in the fit, A_i is the amplitude of a given component, τ_i is the lifetime of a given component, G_R is a Gaussian instrument response function (fixed at 0.5 ps full-width-at-half-maximum), and $\otimes$ represents a convolution. The injection was modeled using a double exponential function, and a third component was added as necessary for trapping.[53] A scaling factor was calculated from the sum of injection component amplitudes, representing the total change in THz amplitude, and was used to normalize the values of A_i. Weighted lifetimes, τ_{inj}, were calculated using the formula $\tau_{inj} = A_1\tau_1 + A_2\tau_2$.

Sensitized SnO_2 samples were prepared as previously described.[54] Briefly, about 4−6 μm thick mesoporous SnO_2 films were treated with a single pulse of TiO_2 by atomic layer deposition (ALD) to passivate any nonmobile surface states.[54] The films were then sensitized by soaking in a 0.5 mM solution of dye in toluene for 4 h at 60 °C, except harsher conditions (16 h at 90 °C) were used for **PhSila**. Films were then sealed in 0.1 M $Na_2SO_{4(aq)}$ (pH 6) between another piece of quartz with a ∼60 μm Surlyn spacer.

Relative injection yields were determined from TRTS measurements from the scaling factor based on a calibration using **RuPhos** on a nominally identical substrate to that used for the porphyrin samples.[55] At pH 6, the injection yield for **RuPhos** on SnO_2 is estimated to be 100%.[54,55] The injection yield, Φ_{inj}, is defined as $\Phi_{inj} = N_e / N_{photon}$, where N_e is the total number of electrons injected into the semiconductor conduction band from dye molecules, and N_{photon} is the total number of photons absorbed by dye molecules. Although we anticipate that N_e is underestimated because of injection into THz-silent states,[54,56] this error should be systematic across all samples and is corrected for by the use of **RuPhos** on identical substrates. The use of a single TiO_2 ALD pulse also helps to passivate nonmobile, THz-silent states.[54,57] Although this has the potential to shift the energy levels of surface states, we expect that this is negligible compared to the mobile states probed by TRTS. Our calibration was constructed by photoexciting a series of **RuPhos** samples at a number of different fluences such that we could control N_{photon}, also ensuring that the loading was high enough that the dependence on N_{photon} was not saturated. From the scaling factor values extracted from the fits, which are proportional to N_e, and by assuming that Φ_{inj} is approximately unity for **RuPhos**, we produced a calibration curve for N_e versus scaling factor with a slope of $(1.47 \pm 0.4) \times 10^{13}$ electrons cm^{-2} (see Figure S4 for the calibration curve). From this calibration curve, we estimate N_e using the scaling factor and N_{photon} by measuring the loading of the porphyrins per unit area (for each linker−anchor combination) compared to the fluence per unit area. With the use of this method, a value for Φ_{inj} relative to **RuPhos** was calculated for all eight porphyrins used in this work.

Nanosecond Transient Absorption (TA) Spectroscopy. SnO_2 films were doctor-bladed on glass using one layer of Scotch Magic Tape as a spacer layer. TA samples were also coated with one pulse of ALD TiO_2. TA measurements were performed using an Edinburgh Instruments LP920 TA spectrometer. Samples were photoexcited at 505 nm (3.82 mJ cm^{-2}) using the output of an OPO (Spectra Physics basiScan M) pumped with the third harmonic of a Nd:YAG laser (Spectra Physics INDI-10). The probe source was a pulsed 450 W Xe arc lamp, which was passed through the sample and detected at 470 nm using a monochromator and photomultiplier tube.

TA traces at a given wavelength were fit with a six-component exponential function with fixed decadic lifetimes going from 0.01 μs to 1 ms. The lifetimes were held constant, and the amplitudes of each component were the fitting parameters. From the lifetimes and corresponding amplitudes, the weighted recombination lifetime, τ_{recomb}, was calculated according to the eq 2 below.

$$\tau_{recomb} = \sum_{i=1}^{n} A_i\tau_i \tag{2}$$

Quantum Chemistry Methods. All eight porphyrin structures were optimized in vacuum using density functional theory (DFT) at the B3LYP[58]/def2SVP[59] level using the Gaussian09 software package.[60] This was followed by frequency calculations to confirm that a stable minimum energy structure had been found for each dye. Single point energy calculations with an implicit water-polarizable continuum solvent[61] were performed to obtain more accurate orbitals and energetics for the species in solvent. Electron density isosurfaces were generated using the GaussView 5 software program.[62] Electron density isosurfaces shown in this work were generated using an isovalue of 0.0025. Potential binding modes for the different anchoring groups were obtained by partial DFT optimization. A phenyl-anchor species for each of the four anchor types was allowed to relax on a 48 atom slab of SnO_2 at the B3LYP[58]/def2SV level. All but the nearest 4 Sn and 9 O atoms were frozen during this partial optimization. Computational costs prohibited the full dye systems from being optimized on the slab.

■ RESULTS AND DISCUSSION

Molecular Designs. In a previous study, we successfully demonstrated the redox tunability of porphyrin photosensitizers by varying the number of electron-withdrawing CF_3 groups on the porphyrin core.[34] Here we adopt the same porphyrin framework with three bis-CF_3-substituted phenyl units, leading to a first oxidative potential of ca. 1.5 V vs NHE. This potential is sufficiently positive to transfer holes to most water-oxidation catalysts.[63,64] This chromophore framework also has an excited-state potential of about −0.4 V vs NHE, offering sufficient driving force for interfacial electron injection

DOI: 10.1021/acs.jpcc.7b12405
J. Phys. Chem. C 2018, 122, 13529−13539

Table 1. Electrochemical and Photophysical Properties of Eight Porphyrins in CH_2Cl_2

porphyrin	abs (nm)	ems (nm)	Φ_f[a]	1st $E_{1/2}$[b] (V vs NHE)	2nd $E_{1/2}$[b] (V vs NHE)	S_1[c] (V vs NHE)
PhCarbEster[d]	418, 513, 547, 588, 644	647, 712	0.066	1.53	1.73	−0.39
PhHydrox	418, 514, 548, 589, 644	647, 711	0.067	1.53	1.74	−0.39
PhPhosEster	418, 512, 547, 588, 644	647, 712	0.065	1.52	1.72	−0.40
PhSila	418, 512, 548, 589, 644	647, 712	0.080	1.44	1.67	−0.48
BzdCarbEster	419, 512, 549, 588, 644	647, 712	0.063	1.58	1.82	−0.34
BzdHydrox	419, 514, 547, 589, 644	647, 712	0.059	1.55	1.76	−0.37
BzdPhosEster	418, 512, 549, 589, 644	647, 712	0.072	1.58	1.79	−0.34
BzdSila	418, 513, 547, 589, 644	647, 711	0.069	1.52	1.71	−0.40

[a]Determined in CH_2Cl_2 relative to that of **PhCarbEster**. [b]Oxidative midpoint potentials determined in 0.1 M $TBAPF_6$ in CH_2Cl_2. [c]Excited-state (S_1) potentials. [d]From ref 34.

into the conduction band of SnO_2 (0.05 V vs NHE, pH 6) from both the S_1 and S_2 excited states. We utilized four of the most widely studied anchoring groups (carboxylate, hydroxamate, phosphonate, and silatrane) in DSSCs and WS-DSPECs and covalently linked them to the porphyrin framework. These anchoring groups are more chemically and electrochemically stable than others, such as catechol and acetylacetonate, which can undergo oxidation and deacetylation, respectively, in aqueous media.[45] We also utilized a pair of linkers with different electronic conjugation and length (phenylene vs benzanilidylene) to connect the porphyrin framework and different anchoring groups (Chart 1). Two of the four anchoring groups are in their protected form. The hydroxamate group is protected by tetrahydropyranyl (THP) to facilitate purification and increase chemical stability, and the THP-protecting group is spontaneously hydrolyzed in situ during deposition on metal oxide surfaces, as we have previously shown.[65] For a silatrane, the siloxane unit, which is vulnerable to oligomerization, is protected with a triethanolamine unit that is removed in situ during deposition.[66]

Photophysical and Electrochemical Properties in Solution. The absorption and fluorescence emission spectra were collected for each target porphyrin or its ester precursor (Table 1). The ester precursors, instead of the acids, were used for studying photophysical and electrochemical properties to preclude possible side effects or side reactions due to the presence or absence of protons, such as aggregation of the porphyrin acids via hydrogen bonding in nonpolar solvents. All eight porphyrins exhibited characteristic porphyrin spectral features, including an intense Soret band absorption at ca. 418 nm and two Q-bands paired with two vibronic bands in the range of 500−700 nm (Figure 1). The fluorescence quantum yields (Φ_f) of these porphyrins were calculated using **PhCarbEster** with a known Φ_f as the reference compound.[34] The spectra of two representative compounds (**PhHydrox** and **BzdHydrox**) are displayed in Figure 1. These nearly identical spectra and similar Φ_f (0.059−0.080) indicate that the variation of linkers and anchoring groups does not significantly alter the electronic structure of the porphyrin core.

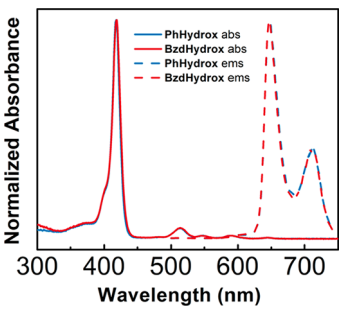

Figure 1. Absorption and fluorescence spectra of two representative porphyrins, **PhHydrox** and **BzdHydrox**, in CH_2Cl_2. The spectra were normalized to their most intense bands.

The electrochemical properties were investigated by cyclic voltammetry (CV), and the half-wave potentials ($E_{1/2}$) of the radical cations and dications are listed in Table 1. Due to the presence of three strong electron-withdrawing bis-CF_3-phenyl substituents, which destabilize the cations, the porphyrins exhibit very high potentials around 1.44−1.58 V vs NHE for the first oxidation and 1.67−1.82 V vs NHE for the second oxidation, corresponding to the radical cation/porphyrin couple and the dication/radical cation couple, respectively. The ground-state potential of **PhSila** is approximately 100 mV lower than the other porphyrins, presumably due to the lower electron-withdrawing ability of the oxo-silyl group compared to the strongly electron-withdrawing carbonyl or phosphonate units for the other seven compounds. While the ground-state potentials for the porphyrin radical cations were obtained from direct CV measurements, the excited-state (S_1) potentials were calculated based on the ground-state potentials and the transition energies, which were extracted from the intersection of the normalized absorption and fluorescence spectra. All the parameters of ground-state and excited-state potentials as well as the conduction band energy level of SnO_2, are depicted in Figure 2. The excited-state potentials of all eight porphyrins lie 0.29−0.43 V higher than the energy of the conduction band of SnO_2, indicating sufficient driving force for IET to SnO_2.

Steady-State Emission Measurements on Metal Oxides. Steady-state emission measurements were performed for all eight CF_3-substituted porphyrins on both SnO_2 and ZrO_2 mesoporous thin films in 0.1 M Na_2SO_4(aq) (pH 6). Because the conduction band edge of ZrO_2 lies well above the S_2 singlet level of the porphyrins, injection into ZrO_2 cannot occur.[67,68] The emission spectra of the porphyrins in addition to bis(2,2′-bipyridine)(4,4′-diphosphonato-2,2′-bipyridine)-ruthenium(II) bis(hexafluorophosphate) (**RuPhos**) on both SnO_2 and ZrO_2 are included in the Supporting Information (SI, Figure S1). **RuPhos** was our reference compound, because it has near unity injection yield on SnO_2 at pH 6,[54,55] serving as a standard for injection yields. From emission measurements, it is seen that **RuPhos** exhibits essentially no emission on SnO_2 and strong emission on ZrO_2, consistent with quantitative injection into SnO_2. The eight porphyrins measured exhibit emission on both ZrO_2 and SnO_2, suggesting injection yields less than unity. However, the emission intensity on SnO_2 is always less than

DOI: 10.1021/acs.jpcc.7b12405
J. Phys. Chem. C 2018, 122, 13529−13539

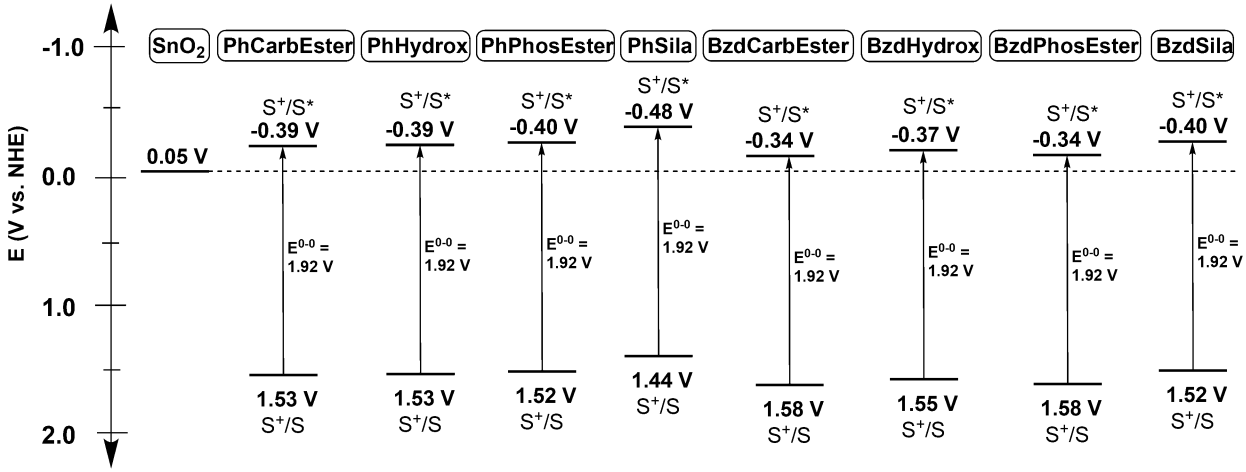

Figure 2. Energy level diagram illustrating the ground- and excited-state (S_1) potentials.

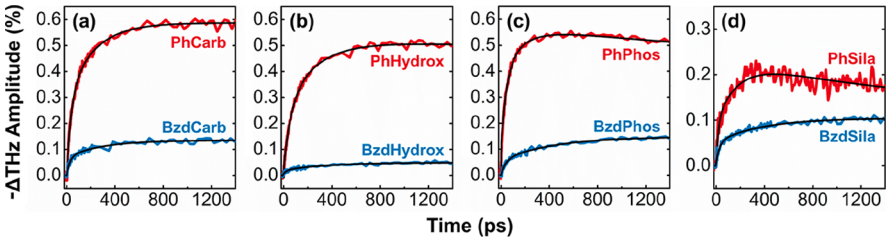

Figure 3. TRTS scans of (a) **Carb**, (b) **Hydrox**, (c) **Phos**, and (d) **Sila** CF_3-substituted porphyrins on SnO_2. Phenylene linker (**Ph**) traces are shown in red, benzanilidylene linker (**Bzd**) traces are shown in blue, and fits using eq 1 are shown in black.

that observed on ZrO_2, implying some degree of electron injection.

Electron-Injection Dynamics and Yield. IET dynamics and injection yields of the eight porphyrins on SnO_2 were studied using TRTS. Because TRTS measurements directly probe mobile electrons in the conduction band, this method provides a more direct measurement of injection yield compared to transient absorption actinometry.[69] THz radiation is attenuated by the presence of mobile electrons in a material, e.g., conduction band electrons in SnO_2, by a process involving excitation of low-energy intraband transitions.[70] TRTS is a valuable spectroscopic tool, because it can interrogate charge carrier dynamics in metal oxides on ultrafast time scales by directly probing the complex permittivity and, therefore, the conductivity of the sample without perturbing the system.[48,49,70] Because conductivity is the product of carrier density and carrier mobility, changes in the amplitude of the THz pulse can be considered proportional to a change in carrier density, assuming that the carrier mobility is constant. Because all porphyrins were deposited on mesoporous, nanoparticulate SnO_2 films with nominally identical particle size, the carrier mobility can be considered constant.[71]

SnO_2 was used exclusively in this work rather than TiO_2 for two primary reasons. First, at pH 6, SnO_2 has a conduction band edge poised at ca. 0.05 V vs NHE, which makes electron injection from both the S_1 and S_2 states of the CF_3-substituted porphyrins energetically favorable, as can be seen in Figure 2. Second, carrier mobility in SnO_2 is much greater than that of TiO_2, which affords a larger attenuation in THz radiation for a given carrier density associated with injected electrons.[71] A single monolayer of TiO_2 was deposited on the surface by atomic layer deposition to passivate nonmobile surface states and give a more accurate injection yield.[54]

Figure 3 shows the TRTS scans for the four anchoring groups studied (**Carb**, **Hydrox**, **Phos**, and **Sila**) with the traces for the phenylene linkers (**Ph**) shown in red and the benzanilidylene linkers (**Bzd**) shown in blue. The TRTS traces were fit with the function described in eq 1 (Experimental Section). Injection was described using two exponential functions, and a third exponential function was included to describe trapping (i.e., electron transfer to low mobility, THz-silent states) as needed. A summary of the fit parameters obtained is presented in Table S1.

Previous work on the injection of electrons from axially bound, T-shaped Zn porphyrins into TiO_2 showed a strong correlation between the electron-injection efficiency as measured by TRTS and the calculated conductivity of the linker−anchor group.[72] Although not directly applicable to the systems studied here, it adds important context to the fundamental experimental result of the study: that the dynamics of electron injection for the porphyrin systems studied here were not significantly different among the anchoring groups investigated. Intuitively, it is expected that the use of a longer linker (**Bzd** instead of **Ph**) should result in lower injection yields as observed, but other clear trends in the dynamics are difficult to infer from the individual injection components.

One readily discernible difference is found in the trapping observed for some of the different linker−anchor combinations. A trapping component was measured in most of the **Ph**−linker samples but was not resolved in half of the **PhCarb** samples. For the **Bzd**−linker samples, a discernible trapping component was only observed in two of the samples (one **BzdHydrox** and one **BzdPhos**). Trapping lifetimes are consistent with each other, which implies that the trapping mechanism is likely a property of the metal oxide,[71] the exception being **PhCarb**, which exhibited a slower trapping lifetime. However, because

DOI: 10.1021/acs.jpcc.7b12405
J. Phys. Chem. C 2018, 122, 13529−13539

the amplitudes of trapping vary greatly, and the dye loading differs, there may be an effect on the surface chemistry of the metal oxide due to the anchoring group, thus facilitating a surface-trapping mechanism.

A more insightful analysis of the injection dynamics comes from the weighted injection lifetimes and the injection yield. Rather than comparing individual components of injection lifetimes, the weighted lifetime, τ_{inj}, provides an appropriate metric for comparison. We found that using linear weighting did not skew τ_{inj} toward long lifetimes, so it was not necessary to use a logarithmic weighting as described by Zhang et al.[73] In previous TRTS studies involving the comparison of different linkers and anchoring groups, only the relative change in THz amplitude was used to quantify relative injection yields among dye photosensitizers.[44,72,74] In this work, we also accounted for the variable dye loading of each porphyrin photosensitizer and calculated the injection yield relative to **RuPhos** based on the procedure discussed in the Experimental Section. A comparison of τ_{inj} and the calculated relative injection yields for all eight porphyrins is shown in Figure 4.

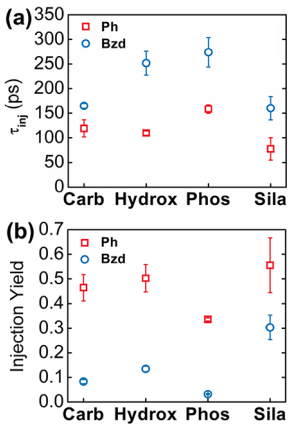

Figure 4. Comparison of (a) τ_{inj} and (b) injection yield of CF_3-substituted porphyrins. Phenylene linkers (**Ph**) are shown in blue, and benzanilidylene linkers (**Bzd**) are shown in red. Uncertainties are the standard error from a set of independent trials.

Comparing the injection dynamics and yield of the porphyrins reveals that while there are some differences, they are relatively small, and no clear trend emerges with respect to the anchoring groups. Increasing the linker length (i.e., **Ph** to **Bzd**) increases the injection lifetime, as expected, by anywhere from 50 to 150 ps, and decreases the injection yield by anywhere from 0.25 to 0.38. Modifying the anchoring group from a phosphonate to a carboxylate to a hydroxamate increases the injection yield as had been previously observed.[72] However, the silatrane injection yield is abnormally high for an anchor thought to have poor electronic coupling similar to phosphonate,[45,75] making a through linker−anchor IET mechanism inconclusive. For the long linkers, it appears that **BzdCarb** and **BzdSila** inject slightly faster than **BzdPhos** and **BzdHydrox**, but this trend is not mirrored in the **Ph** porphyrins, which show much smaller statistically significant differences.

As described in the DFT Calculations section and in previous work,[76,46] IET must proceed either through space directly from a core porphyrin orbital to the metal oxide or through higher excited states (i.e., electron transport orbitals), which are almost entirely localized on the linker−anchor (LUMO+2 for **Carb** and **Hydrox**, LUMO+6 for **Phos**, and LUMO+9 for **Sila**). In the latter case, the electronic coupling between the porphyrin ring and metal oxide orbitals is relatively weak, and the linker−anchor acts as an energetic barrier to electron injection. However, the calculations show that the transport orbitals are energetically inaccessible, and there is no discernible trend between the magnitude of the energetic barrier and τ_{inj}. If the energetic barrier were to mediate IET, it is expected that **Carb** and **Hydrox** would have similar injection lifetimes that are faster than **Phos** and **Sila** as discussed further in the section on DFT Calculations.

Previous work by Ye et al.[46] suggested that IET may occur through space, which would cause injection lifetimes to be dependent on the geometry of the porphyrin adsorbed to the surface, i.e., its distance from the interface, rather than the linker−anchor used. The porphyrins used were functionalized with trimethylphenyl groups at the *meso* positions, rather than the CF_3-substituted phenyl groups used in this work. Specifically, they used polarization-dependent sum frequency generation measurements of a nitrile tag opposite the linker−anchor to determine that the porphyrins used in their study were adsorbed to a TiO_2 surface at tilt angles between 40 to 70°.[46] Therefore, it is reasonable to conclude that the porphyrins used in this work bind to the surface over a similar range of angles, which implies that the through-space distance from the LUMO and LUMO+1 orbitals to acceptor states in the metal oxide is smaller than the through-linker distance. Given that through-linker IET is energetically unfavorable, and the porphyrins adsorb to SnO_2 at an angle, our combined results suggest that injection for these porphyrins likely occurs through-space rather than through the linkers.

The anchoring group typically has an effect on the binding geometry of the linker and can lead to different tilt angles on the surface.[46,77] From the results shown in Figure 4a, it can be inferred that **BzdCarb** and **BzdSila** bind to SnO_2 at larger tilt angles than **BzdHydrox** and **BzdPhos** based on the differences in τ_{inj} (slow injection times imply a small tilt angle). Likewise, the binding geometry of the **Ph**−linker porphyrins is likely very similar due to the smaller range of τ_{inj} values. However, the binding geometry is a notoriously difficult parameter to precisely determine, as it is dependent on a number of factors including dye loading, linker−anchor identity, and dye deposition conditions.[46]

The results shown in Figures 3 and 4 indicate that for longer linkers, there is little benefit to choosing a particular anchoring group, because injection is through space. Injection yields vary by only a factor of ∼0.3 between different linkers and ∼0.3 between different anchors. This is in agreement with previous work by Gust and coworkers, which has shown that porphyrins have comparable performance in DSSCs regardless of linker identity (carboxylate, phosphonate, or silatrane) when the dye loadings are comparable.[75] Choi and coworkers have shown that anchoring group effects can differ depending on the solvation conditions, for both nonaqueous DSSCs[78] or aqueous WS-DSPECs,[79] because this leads to different dielectric environments around the dye−metal oxide interface.[80] The fact that these results agree with those reported by Gust and coworkers suggest that, although the solvent may affect IET dynamics, the mechanism by which IET occurs is dependent on the adsorbed geometry and electronic structure of the photosensitizer.[75]

Other work on DSSCs and WS-DSPECs that assert large differences in performance as a function of anchoring group do

DOI: 10.1021/acs.jpcc.7b12405
J. Phys. Chem. C 2018, 122, 13529−13539

not take into account different surface loading,[44,72,74] which affects the overall number of electrons injected into the metal oxide, or comparison to ruthenium(II) polypyridyl dyes, which have stronger electronic coupling between the metal oxide and MLCT excited state through the anchor and near unity IET efficiency.[81] In dye photosensitizers where IET proceeds through space and the electronic coupling between the dye and metal oxide through the linker−anchor is poor or energetically inaccessible, such as porphyrins, the choice of anchoring group will inevitably have little effect on IET properties unless changes in adsorption geometry are extreme.

Electron Recombination Dynamics. Electron recombination dynamics between SnO_2 and the oxidized dye were monitored using TA spectroscopy. In particular, the peak of the transient absorption feature at 470 nm was monitored,[34] which is a measure of the concentration of the radical cation of the porphyrin.[82] Monitoring the change in absorbance of this feature serves as a good probe for monitoring electron recombination. The dynamics were fit as described in the Experimental Section, and τ_{recomb} values are plotted for the series of eight porphyrins in Figure 5. A summary of representative TA traces and τ_{recomb} values can be found in Figure S2 and Table S2.

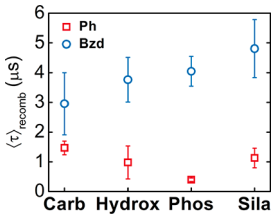

Figure 5. Recombination dynamics for CF_3-substituted porphyrins. Phenylene (**Ph**) linkers are shown in blue, and benzanilidylene linkers (**Bzd**) are shown in red. Uncertainties are the standard error from a set of independent trials.

Although there is a clear difference between **Ph** and **Bzd** recombination lifetimes, it is difficult to extract a statistically significant trend from the different anchoring groups. Statistically insignificant differences among anchoring groups in terms of recombination dynamics have been previously reported,[75] and the difference in terms of the linker is consistent with work performed by Hanson et al.[83] However, **Bzd** is significantly longer that the methylene linker used by Hanson et al., causing a more noticeable effect in τ_{recomb}. The ground-state potentials of all eight porphyrins are within 80 mV of each other, so the thermodynamic driving force is likely not the cause of the substantial increase in τ_{recomb} from **Ph** to **Bzd**. The measured increase in τ_{recomb} from **Ph** to **Bzd** is the result of different linker lengths (see SI for calculated linker lengths), rigidity, and adsorbate tilt angle,[74] which is consistent with our assessment that IET likely proceeds through space.

DFT Calculations. DFT calculations were performed on the porphyrins with phenylene linkers (**Ph**) to investigate the effects of the linker−anchor groups on porphyrin core electronic structure and through-linker IET. DFT calculations of binding geometries are often prohibitively expensive and plagued by metastable geometries, so the calculation of tilt orientations was not performed. The orbital energies and shapes calculated by DFT show that the different anchoring groups have very little effect on the four Gouterman[84] orbitals as would be expected given their distance from the porphyrin core. Figure 6 shows these orbitals for the representative **PhCarb**. In order to investigate the effect that the anchoring

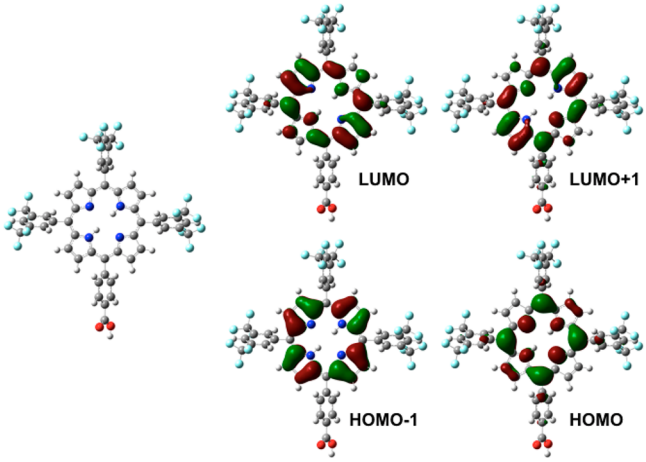

Figure 6. DFT calculated frontier orbitals for the model **PhCarb** porphyrin.

group has on through-linker IET, the virtual orbitals of the **Ph**-series porphyrins were scrutinized in further detail (see Table S3 for the energetics of several orbitals for all four dyes). If IET were to occur through the molecular linkers, the **Bzd**-series porphyrins would follow the same injection trends as the short linker series with the caveat that the longer linkers are further isolated from the anchoring groups, and there are additional unoccupied orbitals spanning the extra length of the linkers.

For porphyrin dyes such as those considered in this study, electronic excitation and subsequent relaxation leaves the excited electron in the degenerate LUMO and LUMO+1 orbitals. Through-linker injection events can then potentially occur through unoccupied π^* orbitals in the linker and into the semiconductor conduction band. For many similar porphyrin dyes,[76] the lowest lying potential transport orbital is the LUMO +2, which tends to be largely localized on the linker and is the most energetically accessible. For the carboxylate and hydroxamate anchoring groups, this trend holds, and through-linker injection would most likely occur through the LUMO+2 orbitals. However, for the silatrane and phosphonate anchoring groups, the lack of an electronegative oxygen atom close to the phenylene ring increases the phenylene π^* orbital energy. Figure 7 shows the lowest lying potential transport orbitals for each of the four dyes, and Table 2 shows the energies of these orbitals relative to their respective LUMO+1 orbitals.

If the transport orbital is approximated as an energetic barrier, higher energies will result in slower and less efficient injection. Though the energy differences in the height of this barrier caused by the different anchoring groups is relatively small, (ca. 0.5 eV in the most extreme case), we would still anticipate observable differences in the injection times and amplitudes. Accordingly, the simplest explanation is that injection is occurring dominantly through space rather than through the molecular linkers. Through-space injection for these porphyrins is consistent with what has previously been reported[46] and is consistent with the high energetic positioning of the DFT-calculated potential transport orbitals (Table 2). Even with photoexcitation at energies 0.5 eV higher than the S_1 state of the dye molecules, it is unlikely that a significant fraction of the excited states will be able to reach the transport

DOI: 10.1021/acs.jpcc.7b12405
J. Phys. Chem. C 2018, 122, 13529−13539

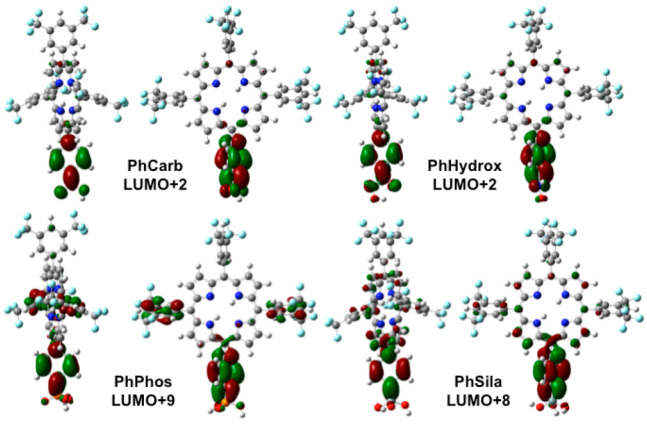

Figure 7. DFT calculated virtual orbitals localized to the linker and anchoring group for each of the phenylene-linked dyes. These linker π^* orbitals are the most likely candidates for through-linker IET.

Table 2. Calculated Energetic Positions (in eV) of the Linker π^* Orbitals relative to the LUMO+1 Orbital (0 eV)

anchors	"transport" orbital 1	"transport" orbital 2
Carboxylate	1.23	---
Hydroxamate	1.31	---
Phosphonate	1.47	1.69
Silatrane	1.77	1.85

orbitals identified via DFT, all of which are at least 1.20 eV higher than the excited-state energy. Further, no trend is observed between the energetic positioning of these transport orbitals and the electron-injection rates. That these results have been observed for two different bridge types and four different anchor types suggests that injection occurs predominantly through space rather than through the linker group.

CONCLUSION

A series of eight novel high-potential porphyrins were synthesized, and their IET to SnO_2 was studied by a combination of spectroscopic techniques and DFT calculations. The effect of linker (**Ph** and **Bzd**) and anchoring group (**Carb**, **Hydrox**, **Phos**, and **Sila**) on IET in this series of CF_3-substituted porphyrins was investigated and determined to have less impact than for molecular assemblies where IET is through the linker/anchor. Unsurprisingly, the electrochemical and photophysical properties of the porphyrins did not differ significantly as a function of linker and anchoring group.

This study suggests direct, through-space IET occurs rather than electron transfer through the linker for this particular set of linkers and anchoring groups. The conventional understanding in dye photosensitizer design posits that the anchoring group plays a large role in IET properties, but our spectroscopic and computational results suggest that there is little difference in IET among our porphyrin photosensitizer systems with different anchoring groups.

Because the different anchoring groups affect dye loading on SnO_2, we calculated injection yields relative to **RuPhos** based on TRTS measurements, thereby taking into account dye loadings. This new methodology provides a direct measure of injection yield with respect to mobile conduction band electrons and serves as an alternative to TA actinometry.[69] In addition, injection dynamics (τ_{inj}) determined from TRTS and recombination dynamics (τ_{recomb}) determined from TA showed insignificant differences in lifetimes between anchoring groups. Some appreciable differences were apparent in trapping dynamics, but this is likely attributed to changes in surface chemistry caused by the anchoring group.

We explain these phenomena by considering the electronic structure using DFT calculations of the porphyrins synthesized in this work. These calculations show that if the injection were occurring through the molecular linker groups, a significant difference in injection and recombination lifetimes would be expected. The through-linker transport orbitals (at LUMO+2 for **PhCarb** and **PhHydrox**, LUMO+6 for **PhPhos**, and LUMO +9 for **PhSila**) are shown to be 1.2−1.8 eV above the LUMO +1 orbital, further suggesting the unlikely possibility of through-linker injection.

In light of these results, we suggest that the anchoring groups of porphyrin photosensitizers that inject through space should be chosen based primarily on stability and synthetic viability, bypassing the challenge of energy level alignment. Although through-space injection could be less efficient than injection through the molecular linker, it might simplify the rational design of dye photosensitizers for constructing stable WS-DSPECs and related photoelectrochemical cells.

ASSOCIATED CONTENT

Supporting Information

The Supporting Information is available free of charge on the ACS Publications website at DOI: 10.1021/acs.jpcc.7b12405.

> Emission spectra of eight porphyrins and **RuPhos** on SnO_2 and ZrO_2, fit parameters from TRTS results, representative TA spectroscopy results, **Ph** porphyrin orbital energies, determination of dye loading and results on SnO_2, N_e vs scaling factor calibration curve, TRTS power dependence measurements of **RuPhos** and fit parameters, synthesis and characterization of the eight porphyrins (PDF)

AUTHOR INFORMATION

Corresponding Authors

*E-mail: robert.crabtree@yale.edu (R.H.C.)
*E-mail: victor.batista@yale.edu (V.S.B.)
*E-mail: charles.schmuttenmaer@yale.edu (C.A.S.)
*E-mail: gary.brudvig@yale.edu (G.W.B.)

ORCID

John R. Swierk: 0000-0001-5811-7285
Adam J. Matula: 0000-0002-1241-2470
Kevin P. Regan: 0000-0003-3522-092X
Robert H. Crabtree: 0000-0002-6639-8707
Victor S. Batista: 0000-0002-3262-1237
Charles A. Schmuttenmaer: 0000-0001-9992-8578
Gary W. Brudvig: 0000-0002-7040-1892

Present Address

‡For B.J.B.: Division of Chemistry and Chemical Engineering, California Institute of Technology, Pasadena, CA 91125, United States

Author Contributions

†J.J. and J.A.S. contributed equally.

Notes

The authors declare no competing financial interest.

DOI: 10.1021/acs.jpcc.7b12405
J. Phys. Chem. C 2018, 122, 13529−13539

■ ACKNOWLEDGMENTS

This work was supported by the U.S. Department of Energy, Chemical Sciences, Geosciences, and Biosciences Division, Office of Basic Energy Sciences, Office of Science (Grant DEFG02-07ER15909). Additional support was provided by a generous donation from the TomKat Charitable Trust. A.J.M. was supported by the National Science Foundation Graduate Research Fellowship under Grant No. DGE-1122492. We thank the staff at Yale West Campus Analytical Core and Yale WM Keck Foundation Biotechnology Resource Laboratory for their help with instrumentation. J.A.S., J.R.S., and C.A.S. would like to thank Prof. Jason Baxter and Siming Li at Drexel University for allowing us to run an experiment while our spectrometer was being repaired. V.S.B. acknowledges computational time from NERSC and Yale HPC.

■ REFERENCES

(1) Lewis, N. S. Toward Cost-Effective Solar Energy Use. *Science* **2007**, *315*, 798−801.

(2) Chapin, D. M.; Fuller, C. S.; Pearson, G. L. A New Silicon p-n Junction Photocell for Converting Solar Radiation into Electrical Power. *J. Appl. Phys.* **1954**, *25*, 676−677.

(3) Battaglia, C.; Cuevas, A.; De Wolf, S. High-Efficiency Crystalline Silicon Solar Cells: Status and Perspectives. *Energy Environ. Sci.* **2016**, *9*, 1552−1576.

(4) O'Regan, B.; Grätzel, M. A Low-Cost, High-Efficiency Solar Cell Based on Dye-Sensitized Colloidal TiO_2 Films. *Nature* **1991**, *353*, 737−740.

(5) Hagfeldt, A.; Boschloo, G.; Sun, L.; Kloo, L.; Pettersson, H. Dye-Sensitized Solar Cells. *Chem. Rev.* **2010**, *110*, 6595−6663.

(6) Fan, K.; Yu, J.; Ho, W. Improving Photoanodes to Obtain Highly Efficient Dye-Sensitized Solar Cells: A Brief Review. *Mater. Horiz.* **2017**, *4*, 319−344.

(7) Kojima, A.; Teshima, K.; Shirai, Y.; Miyasaka, T. Organometal Halide Perovskites as Visible-Light Sensitizers for Photovoltaic Cells. *J. Am. Chem. Soc.* **2009**, *131*, 6050−6051.

(8) Zhang, W.; Eperon, G. E.; Snaith, H. J. Metal Halide Perovskites for Energy Applications. Nat. *Energy* **2016**, *1*, 16048.

(9) Yang, S.; Fu, W.; Zhang, Z.; Chen, H.; Li, C.-Z. Recent Advances in Perovskite Solar Cells: Efficiency, Stability and Lead-Free Perovskite. *J. Mater. Chem. A* **2017**, *5*, 11462−11482.

(10) Gray, H. B. Powering the Planet with Solar Fuel. *Nat. Chem.* **2009**, *1*, 7.

(11) Concepcion, J. J.; House, R. L.; Papanikolas, J. M.; Meyer, T. J. Chemical Approaches to Artificial Photosynthesis. *Proc. Natl. Acad. Sci. U. S. A.* **2012**, *109*, 15560−15564.

(12) Nocera, D. G. Solar Fuels and Solar Chemicals Industry. *Acc. Chem. Res.* **2017**, *50*, 616−619.

(13) Young, K. J.; Martini, L. A.; Milot, R. L.; Snoeberger, R. C., III; Batista, V. S.; Schmuttenmaer, C. A.; Crabtree, R. H.; Brudvig, G. W. Light-Driven Water Oxidation for Solar Fuels. *Coord. Chem. Rev.* **2012**, *256*, 2503−2520.

(14) Fujishima, A.; Honda, K. Electrochemical Photolysis of Water at a Semiconductor Electrode. *Nature* **1972**, *238*, 37−38.

(15) Walter, M. G.; Warren, E. L.; McKone, J. R.; Boettcher, S. W.; Mi, Q.; Santori, E. A.; Lewis, N. S. Solar Water Splitting Cells. *Chem. Rev.* **2010**, *110*, 6446−6473.

(16) Jiang, C.; Moniz, S. J. A.; Wang, A.; Zhang, T.; Tang, J. Photoelectrochemical Devices for Solar Water Splitting - Materials and Challenges. *Chem. Soc. Rev.* **2017**, *46*, 4645−4660.

(17) White, J. L.; Baruch, M. F.; Pander, J. E., III; Hu, Y.; Fortmeyer, I. C.; Park, J. E.; Zhang, T.; Liao, K.; Gu, J.; Yan, Y.; et al. Light-Driven Heterogeneous Reduction of Carbon Dioxide: Photocatalysts and Photoelectrodes. *Chem. Rev.* **2015**, *115*, 12888−12935.

(18) Qiao, J.; Liu, Y.; Hong, F.; Zhang, J. A Review of Catalysts for the Electroreduction of Carbon Dioxide to Produce Low-Carbon Fuels. *Chem. Soc. Rev.* **2014**, *43*, 631−675.

(19) Youngblood, W. J.; Lee, S. H.; Kobayashi, Y.; Hernandez-Pagan, E. A.; Hoertz, P. G.; Moore, T. A.; Moore, A. L.; Gust, D.; Mallouk, T. E. Photoassisted Overall Water Splitting in a Visible Light-Absorbing Dye-Sensitized Photoelectrochemical Cell. *J. Am. Chem. Soc.* **2009**, *131*, 926−927.

(20) Swierk, J. R.; Mallouk, T. E. Design and Development of Photoanodes for Water-Splitting Dye-Sensitized Photoelectrochemical Cells. *Chem. Soc. Rev.* **2013**, *42*, 2357−2387.

(21) Xu, P.; McCool, N. S.; Mallouk, T. E. Water Splitting Dye-Sensitized Solar Cells. *Nano Today* **2017**, *14*, 42−58.

(22) Li, F.; Fan, K.; Xu, B.; Gabrielsson, E.; Daniel, Q.; Li, L.; Sun, L. Organic Dye-Sensitized Tandem Photoelectrochemical Cell for Light Driven Total Water Splitting. *J. Am. Chem. Soc.* **2015**, *137*, 9153−9159.

(23) Sheridan, M. V.; Hill, D. J.; Sherman, B. D.; Wang, D.; Marquard, S. L.; Wee, K. R.; Cahoon, J. F.; Meyer, T. J. All-in-One Derivatized Tandem p+n-Silicon-SnO_2/TiO_2 Water Splitting Photoelectrochemical Cell. *Nano Lett.* **2017**, *17*, 2440−2446.

(24) Brown, A. M.; Antila, L. J.; Mirmohades, M.; Pullen, S.; Ott, S.; Hammarström, L. Ultrafast Electron Transfer between Dye and Catalyst on a Mesoporous NiO Surface. *J. Am. Chem. Soc.* **2016**, *138*, 8060−8063.

(25) Queyriaux, N.; Wahyuono, R. A.; Fize, J.; Gablin, C.; Wachtler, M.; Martinez, E.; Leonard, D.; Dietzek, B.; Artero, V.; Chavarot-Kerlidou, M. Aqueous Photocurrent Measurements Correlated to Ultrafast Electron Transfer Dynamics at Ruthenium Tris Diimine-Sensitized NiO Photocathodes. *J. Phys. Chem. C* **2017**, *121*, 5891−5904.

(26) Symes, M. D.; Lutterman, D. A.; Teets, T. S.; Anderson, B. L.; Breen, J. J.; Nocera, D. G. Photo-Active Cobalt Cubane Model of an Oxygen-Evolving Catalyst. *ChemSusChem* **2013**, *6*, 65−69.

(27) Brennan, B. J.; Durrell, A. C.; Koepf, M.; Crabtree, R. H.; Brudvig, G. W. Towards Multielectron Photocatalysis: A Porphyrin Array for Lateral Hole Transfer and Capture on a Metal Oxide Surface. *Phys. Chem. Chem. Phys.* **2015**, *17*, 12728−12734.

(28) Brennan, B. J.; Regan, K. P.; Durrell, A. C.; Schmuttenmaer, C. A.; Brudvig, G. W. Solvent Dependence of Lateral Charge Transfer in a Porphyrin Monolayer. *ACS Energy Lett.* **2017**, *2*, 168−173.

(29) Muuronen, M.; Parker, S. M.; Berardo, E.; Le, A.; Zwijnenburg, M. A.; Furche, F. Mechanism of Photocatalytic Water Oxidation on Small TiO_2 Nanoparticles. *Chem. Sci.* **2017**, *8*, 2179−2183.

(30) Bella, F.; Gerbaldi, C.; Barolo, C.; Grätzel, M. Aqueous Dye-Sensitized Solar Cells. *Chem. Soc. Rev.* **2015**, *44*, 3431−3473.

(31) Moore, G. F.; Konezny, S. J.; Song, H.-e.; Milot, R. L.; Blakemore, J. D.; Lee, M. L.; Batista, V. S.; Schmuttenmaer, C. A.; Crabtree, R. H.; Brudvig, G. W. Bioinspired High-Potential Porphyrin Photoanodes. *J. Phys. Chem. C* **2012**, *116*, 4892−4902.

(32) Swierk, J. R.; Mendez-Hernandez, D. D.; McCool, N. S.; Liddell, P.; Terazono, Y.; Pahk, I.; Tomlin, J. J.; Oster, N. V.; Moore, T. A.; Moore, A. L.; Gust, D.; Mallouk, T. E. Metal-Free Organic Sensitizers for Use in Water-Splitting Dye-Sensitized Photoelectrochemical Cells. *Proc. Natl. Acad. Sci. U. S. A.* **2015**, *112*, 1681−1686.

(33) Brennan, B. J.; Lam, Y. C.; Kim, P. M.; Zhang, X.; Brudvig, G. W. Photoelectrochemical Cells Utilizing Tunable Corroles. *ACS Appl. Mater. Interfaces* **2015**, *7*, 16124−16130.

(34) Jiang, J.; Swierk, J. R.; Materna, K. L.; Hedström, S.; Lee, S. H.; Crabtree, R. H.; Schmuttenmaer, C. A.; Batista, V. S.; Brudvig, G. W. High-Potential Porphyrins Supported on SnO_2 and TiO_2 Surfaces for Photoelectrochemical Applications. *J. Phys. Chem. C* **2016**, *120*, 28971−28982.

(35) Urbani, M.; Grätzel, M.; Nazeeruddin, M. K.; Torres, T. Meso-Substituted Porphyrins for Dye-Sensitized Solar Cells. *Chem. Rev.* **2014**, *114*, 12330−12396.

(36) Lindsey, J. S. Synthetic Routes to Meso-Patterned Porphyrins. *Acc. Chem. Res.* **2010**, *43*, 300−311.

(37) Laha, J. K.; Dhanalekshmi, S.; Taniguchi, M.; Ambroise, A.; Lindsey, J. S. A Scalable Synthesis of Meso-Substituted Dipyrromethanes. *Org. Process Res. Dev.* **2003**, *7*, 799−812.

(38) Antoniuk-Pablant, A.; Terazono, Y.; Brennan, B. J.; Sherman, B. D.; Megiatto, J. D.; Brudvig, G. W.; Moore, A. L.; Moore, T. A.; Gust,

DOI: 10.1021/acs.jpcc.7b12405
J. Phys. Chem. C 2018, 122, 13529−13539

D. A New Method for the Synthesis of β-Cyano Substituted Porphyrins and Their Use as Sensitizers in Photoelectrochemical Devices. *J. Mater. Chem. A* **2016**, *4*, 2976−2985.
(39) Holten, D.; Bocian, D. F.; Lindsey, J. S. Probing Electronic Communication in Covalently Linked Multiporphyrin Arrays. A Guide to the Rational Design of Molecular Photonic Devices. *Acc. Chem. Res.* **2002**, *35*, 57−69.
(40) Mandal, A. K.; Sahin, T.; Liu, M.; Lindsey, J. S.; Bocian, D. F.; Holten, D. Photophysical Comparisons of PEGylated Porphyrins, Chlorins and Bacteriochlorins in Water. *New J. Chem.* **2016**, *40*, 9648−9656.
(41) Liu, M.; Chen, C. Y.; Mandal, A. K.; Chandrashaker, V.; Evans-Storms, R. B.; Pitner, J. B.; Bocian, D. F.; Holten, D.; Lindsey, J. S. Bioconjugatable, PEGylated Hydroporphyrins for Photochemistry and Photomedicine. Narrow-Band, Red-Emitting Chlorins. *New J. Chem.* **2016**, *40*, 7721−7740.
(42) Zhang, L.; Cole, J. M. Anchoring Groups for Dye-Sensitized Solar Cells. *ACS Appl. Mater. Interfaces* **2015**, *7*, 3427−3455.
(43) Brennan, B. J.; Keirstead, A. E.; Liddell, P. A.; Vail, S. A.; Moore, T. A.; Moore, A. L.; Gust, D. 1-(3′-Amino)propylsilatrane Derivatives as Covalent Surface Linkers to Nanoparticulate Metal Oxide Films for Use in Photoelectrochemical Cells. *Nanotechnology* **2009**, *20*, 505203.
(44) Martini, L. A.; Moore, G. F.; Milot, R. L.; Cai, L. Z.; Sheehan, S. W.; Schmuttenmaer, C. A.; Brudvig, G. W.; Crabtree, R. H. Modular Assembly of High-Potential Zinc Porphyrin Photosensitizers Attached to TiO_2 with a Series of Anchoring Groups. *J. Phys. Chem. C* **2013**, *117*, 14526−14533.
(45) Materna, K. L.; Crabtree, R. H.; Brudvig, G. W. Anchoring Groups for Photocatalytic Water Oxidation on Metal Oxide Surfaces. *Chem. Soc. Rev.* **2017**, *46*, 6099−6110.
(46) Ye, S.; Kathiravan, A.; Hayashi, H.; Tong, Y.; Infahsaeng, Y.; Chabera, P.; Pascher, T.; Yartsev, A. P.; Isoda, S.; Imahori, H.; Sundström, V. Role of Adsorption Structures of Zn-Porphyrin on TiO_2 in Dye-Sensitized Solar Cells Studied by Sum Frequency Generation Vibrational Spectroscopy and Ultrafast Spectroscopy. *J. Phys. Chem. C* **2013**, *117*, 6066−6080.
(47) Brennan, B. J.; Gust, D.; Brudvig, G. W. Organosilatrane Building Blocks. *Tetrahedron Lett.* **2014**, *55*, 1062−1064.
(48) Beard, M. C.; Turner, G. M.; Schmuttenmaer, C. A. Transient Photoconductivity in GaAs as Measured by Time-Resolved Terahertz Spectroscopy. *Phys. Rev. B: Condens. Matter Mater. Phys.* **2000**, *62*, 15764−15777.
(49) Schmuttenmaer, C. A. Exploring Dynamics in the Far-Infrared with Terahertz Spectroscopy. *Chem. Rev.* **2004**, *104*, 1759−1779.
(50) Cook, D. J.; Hochstrasser, R. M. Intense Terahertz Pulses by Four-Wave Rectification in Air. *Opt. Lett.* **2000**, *25*, 1210−1212.
(51) Bartel, T.; Gaal, P.; Reimann, K.; Woerner, M.; Elsaesser, T. Generation of Single-Cycle THz Transients with High Electric-Field Amplitudes. *Opt. Lett.* **2005**, *30*, 2805−2807.
(52) Wu, Q.; Zhang, X. C. Free-Space Electro-Optic Sampling of Terahertz Beams. *Appl. Phys. Lett.* **1995**, *67*, 3523−3525.
(53) Milot, R. L.; Moore, G. F.; Crabtree, R. H.; Brudvig, G. W.; Schmuttenmaer, C. A. Electron Injection Dynamics from Photoexcited Porphyrin Dyes into SnO_2 and TiO_2 nanoparticles. *J. Phys. Chem. C* **2013**, *117*, 21662−21670.
(54) Swierk, J. R.; McCool, N. S.; Nemes, C. T.; Mallouk, T. E.; Schmuttenmaer, C. A. Ultrafast Electron Injection Dynamics of Photoanodes for Water-Splitting Dye-Sensitized Photoelectrochemical Cells. *J. Phys. Chem. C* **2016**, *120*, 5940−5948.
(55) Gillaizeau-Gauthier, I.; Odobel, F.; Alebbi, M.; Argazzi, R.; Costa, E.; Bignozzi, C. A.; Qu, P.; Meyer, G. J. Phosphonate-Based Bipyridine Dyes for Stable Photovoltaic Devices. *Inorg. Chem.* **2001**, *40*, 6073−6079.
(56) McCool, N. S.; Swierk, J. R.; Nemes, C. T.; Saunders, T. P.; Schmuttenmaer, C. A.; Mallouk, T. E. Proton-Induced Trap States, Injection and Recombination Dynamics in Water-Splitting Dye-Sensitized Photoelectrochemical Cells. *ACS Appl. Mater. Interfaces* **2016**, *8*, 16727−16735.
(57) Prasittichai, C.; Avila, J. R.; Farha, O. K.; Hupp, J. T. Systematic Modulation of Quantum (Electron) Tunneling Behavior by Atomic Layer Deposition on Nanoparticulate SnO_2 and TiO_2 Photoanodes. *J. Am. Chem. Soc.* **2013**, *135*, 16328−16331.
(58) Becke, A. D. Density-Functional Thermochemistry. III. The Role of Exact Exchange. *J. Chem. Phys.* **1993**, *98*, 5648−5652.
(59) Weigend, F. Accurate Coulomb-Fitting Basis Sets for H to Rn. *Phys. Chem. Chem. Phys.* **2006**, *8*, 1057−1065.
(60) Frisch, M. J.; Trucks, G. W.; Schlegel, H. B.; Scuseria, G. E.; Robb, M. A.; Cheeseman, J. R.; Scalmani, G.; Barone, V.; Mennucci, B.; Petersson, G. A.; Nakatsuji, H.; Caricato, M.; Li, X.; Hratchian, H. P.; Izmaylov, A. F.; Bloino, J.; Zheng, G.; Sonnenberg, J. L.; Hada, M.; Ehara, M.; Toyota, K.; Fukuda, R.; Hasegawa, J.; Ishida, M.; Nakajima, T.; Honda, Y.; Kitao, O.; Nakai, H.; Vreven, T.; Montgomery, J. A., Jr.; Peralta, J. E.; Ogliaro, F.; Bearpark, M.; Heyd, J. J.; Brothers, E.; Kudin, K. N.; Staroverov, V. N.; Kobayashi, R.; Normand, J.; Raghavachari, K.; Rendell, A.; Burant, J. C.; Iyengar, S. S.; Tomasi, J.; Cossi, M.; Rega, N.; Millam, J. M.; Klene, M.; Knox, J. E.; Cross, J. B.; Bakken, V.; Adamo, C.; Jaramillo, J.; Gomperts, R.; Stratmann, R. E.; Yazyev, O.; Austin, A. J.; Cammi, R.; Pomelli, C.; Ochterski, J. W.; Martin, R. L.; Morokuma, K.; Zakrzewski, V. G.; Voth, G. A.; Salvador, P.; Dannenberg, J. J.; Dapprich, S.; Daniels, A. D.; Farkas, O.; Foresman, J. B.; Ortiz, J. V.; Cioslowski, J.; Fox, D. J. *Gaussian 09*, revision D.01; Gaussian, Inc.: Wallingford, CT, 2009.
(61) Marenich, A. V.; Cramer, C. J.; Truhlar, D. G. Universal Solvation Model Based on Solute Electron Density and on a Continuum Model of the Solvent Defined by the Bulk Dielectric Constant and Atomic Surface Tensions. *J. Phys. Chem. B* **2009**, *113*, 6378−6396.
(62) *GaussView*, Version 5, Dennington, R.; Keith, T. A.; Millam, J. M., Semichem Inc., Shawnee Mission, KS, 2016.
(63) Tong, L.; Thummel, R. P. Mononuclear Ruthenium Polypyridine Complexes That Catalyze Water Oxidation. *Chem. Sci.* **2016**, *7*, 6591−6603.
(64) Mognon, L.; Mandal, S.; Castillo, C. E.; Fortage, J.; Molton, F.; Aromí, G.; Benet-Buchhlolz, J.; Collomb, M.-N.; Llobet, A. Synthesis, Structure, Spectroscopy and Reactivity of New Heterotrinuclear Water Oxidation Catalysts. *Chem. Sci.* **2016**, *7*, 3304−3312.
(65) Brennan, B. J.; Koenigsmann, C.; Materna, K. L.; Kim, P. M.; Koepf, M.; Crabtree, R. H.; Schmuttenmaer, C. A.; Brudvig, G. W. Surface-Induced Deprotection of THP-Protected Hydroxamic Acids on Titanium Dioxide. *J. Phys. Chem. C* **2016**, *120*, 12495−12502.
(66) Materna, K. L.; Rudshteyn, B.; Brennan, B. J.; Kane, M. H.; Bloomfield, A. J.; Huang, D. L.; Shopov, D. Y.; Batista, V. S.; Crabtree, R. H.; Brudvig, G. W. Heterogenized Iridium Water-Oxidation Catalyst from a Silatrane Precursor. *ACS Catal.* **2016**, *6*, 5371−5377.
(67) Koops, S. E.; Durrant, J. R. Transient Emission Studies of Electron Injection in Dye Sensitised Solar Cells. *Inorg. Chim. Acta* **2008**, *361*, 663−670.
(68) Koops, S. E.; O'Regan, B. C.; Barnes, P. R.; Durrant, J. R. Parameters Influencing the Efficiency of Electron Injection in Dye-Sensitized Solar Cells. *J. Am. Chem. Soc.* **2009**, *131*, 4808−4818.
(69) Bergeron, B. V.; Kelly, C. A.; Meyer, G. J. Thin Film Actinometers for Transient Absorption Spectroscopy: Applications to Dye-Sensitized Solar Cells. *Langmuir* **2003**, *19*, 8389−8394.
(70) Baxter, J. B.; Richter, C.; Schmuttenmaer, C. A. Ultrafast Carrier Dynamics in Nanostructures for Solar Fuels. *Annu. Rev. Phys. Chem.* **2014**, *65*, 423−447.
(71) Regan, K. P.; Swierk, J. R.; Neu, J.; Schmuttenmaer, C. A. Frequency-Dependent Terahertz Transient Photoconductivity of Mesoporous SnO_2 Films. *J. Phys. Chem. C* **2017**, *121*, 15949−15956.
(72) Negre, C. F. A.; Milot, R. L.; Martini, L. A.; Ding, W.; Crabtree, R. H.; Schmuttenmaer, C. A.; Batista, V. S. Efficiency of Interfacial Electron Transfer from Zn-Porphyrin Dyes into TiO_2 Correlated to the Linker Single Molecule Conductance. *J. Phys. Chem. C* **2013**, *117*, 24462−24470.
(73) Zhang, L.; Favereau, L.; Farre, Y.; Mijangos, E.; Pellegrin, Y.; Blart, E.; Odobel, F.; Hammarström, L. Ultrafast and Slow Charge

DOI: 10.1021/acs.jpcc.7b12405
J. Phys. Chem. C 2018, 122, 13529−13539

Recombination Dynamics of Diketopyrrolopyrrole-NiO Dye Sensitized Solar Cells. *Phys. Chem. Chem. Phys.* **2016**, *18*, 18515−18527.
(74) Jiang, J.; Swierk, J. R.; Hedström, S.; Matula, A. J.; Crabtree, R. H.; Batista, V. S.; Schmuttenmaer, C. A.; Brudvig, G. W. Molecular Design of Light-Harvesting Photosensitizers: Effect of Varied Linker Conjugation on Interfacial Electron Transfer. *Phys. Chem. Chem. Phys.* **2016**, *18*, 18678−18682.
(75) Brennan, B. J.; Llansola Portoles, M. J.; Liddell, P. A.; Moore, T. A.; Moore, A. L.; Gust, D. Comparison of Silatrane, Phosphonic Acid, and Carboxylic Acid Functional Groups for Attachment of Porphyrin Sensitizers to TiO_2 in Photoelectrochemical Cells. *Phys. Chem. Chem. Phys.* **2013**, *15*, 16605−16614.
(76) Lee, S.; Regan, K. P.; Hedström, S.; Matula, A. J.; Chaudhuri, S.; Crabtree, R. H.; Batista, V. S.; Schmuttenmaer, C. A.; Brudvig, G. W. Linker Length-Dependent Electron-Injection Dynamics of Trimesitylporphyrins on SnO_2 Films. *J. Phys. Chem. C* **2017**, *121*, 22690−22699.
(77) Ambrosio, F.; Martsinovich, N.; Troisi, A. What Is the Best Anchoring Group for a Dye in a Dye-Sensitized Solar Cell? *J. Phys. Chem. Lett.* **2012**, *3*, 1531−1535.
(78) Park, H.; Bae, E.; Lee, J. J.; Park, J.; Choi, W. Effect of the Anchoring Group in Ru-Bipyridyl Sensitizers on the Photoelectrochemical Behavior of Dye-Sensitized TiO_2 Electrodes: Carboxylate Versus Phosphonate Linkages. *J. Phys. Chem. B* **2006**, *110*, 8740−8749.
(79) Bae, E.; Choi, W. Effect of the Anchoring Group (Carboxylate vs Phosphonate) in Ru-Complex-Sensitized TiO_2 on Hydrogen Production under Visible Light. *J. Phys. Chem. B* **2006**, *110*, 14792−14799.
(80) She, C.; Guo, J.; Lian, T. Comparison of Electron Injection Dynamics from Re-Bipyridyl Complexes to TiO_2 Nanocrystalline Thin Films in Different Solvent Environments. *J. Phys. Chem. B* **2007**, *111*, 6903−6912.
(81) Lundqvist, M. J.; Nilsing, M.; Lunell, S.; Åkermark, B.; Persson, P. Spacer and Anchor Effects on the Electronic Coupling in Ruthenium-Bis-Terpyridine Dye-Sensitized TiO_2 Nanocrystals Studied by DFT. *J. Phys. Chem. B* **2006**, *110*, 20513−20525.
(82) Nayak, A.; Knauf, R. R.; Hanson, K.; Alibabaei, L.; Concepcion, J. J.; Ashford, D. L.; Dempsey, J. L.; Meyer, T. J. Synthesis and Photophysical Characterization of Porphyrin and Porphyrin−Ru(II) Polypyridyl Chromophore−Catalyst Assemblies on Mesoporous Metal Oxides. *Chem. Sci.* **2014**, *5*, 3115−3119.
(83) Hanson, K.; Brennaman, M. K.; Ito, A.; Luo, H.; Song, W.; Parker, K. A.; Ghosh, R.; Norris, M. R.; Glasson, C. R. K.; Concepcion, J. J.; Lopez, R.; Meyer, T. J. Structure−Property Relationships in Phosphonate-Derivatized, Ru^{II} Polypyridyl Dyes on Metal Oxide Surfaces in an Aqueous Environment. *J. Phys. Chem. C* **2012**, *116*, 14837−14847.
(84) Gouterman, M.; Wagnière, G. H.; Snyder, L. C. Spectra of Porphyrins. *J. Mol. Spectrosc.* **1963**, *11*, 108−127.

DOI: 10.1021/acs.jpcc.7b12405
J. Phys. Chem. C 2018, 122, 13529−13539